Journal of Civil Structural Health Monitoring (2024) 14:121–142
https://doi.org/10.1007/s13349-023-00709-1

ORIGINAL PAPER

Ambient vibrations-supported seismic assessment of the Saint Lawrence Cathedral's bell tower in Genoa, Italy

Stefania Degli Abbati[1] · **Daniele Sivori**[1] · **Serena Cattari**[1] · **Sergio Lagomarsino**[1]

Received: 12 December 2022 / Accepted: 16 May 2023 / Published online: 7 June 2023

Abstract
Post-earthquake damage surveys systematically highlight the seismic vulnerability of monumental structures, calling for simple assessment procedures to address the design of effective retrofitting interventions. The structural complexity characterizing monumental structures, however, makes a reliable prediction of their seismic response a relevant challenge of engineering interest. Ambient vibration tests (AVTs) provide valuable support to achieve such a task, improving the knowledge of the actual dynamic behavior of the structure and, consequently, the reliability of the seismic assessment. In this context, the paper illustrates the integration of AVTs outcomes with the evaluation of the seismic performance of historic masonry structures by presenting the comprehensive application to a case study, the bell tower of the Saint Lawrence's Cathedral in Genoa, Italy. The research combines the assessment of the global seismic response of the tower, investigated through a simplified mechanical model, with the local verification of the pinnacles placed at its top, referring to a displacement-based approach on a macro-block model. An extensive ambient vibrations measurement campaign carried out in May 2020 allowed for a comprehensive operational identification of the bell tower and its pinnacles, clarifying the ongoing dynamic interaction with the main body of the church. This valuable information was successfully employed, first, to accurately reproduce the actual constraint conditions induced by the church on the bell tower, a determining factor in the modeling of its global seismic response and, second, to reliably quantify the seismic amplification caused by the tower filtering effect to be used as the seismic input for the local verification of the pinnacles.

Keywords Heritage masonry structures · Monumental church · Dynamic identification · Seismic assessment · Floor spectra

1 Introduction

The vast cultural value encompassed by the historic built heritage is being increasingly recognized by today's society, which strongly demands its preservation for future generations. From an engineering viewpoint, such a value lies not only in the beauty of the architecture and artistic artifacts but equally in the technical and structural solutions inherited from past builders. It is through in-depth and comprehensive knowledge of existing structures, that engineers should pursue their protection and conservation. The task is undoubtedly challenging, considering that historic structures were often built according to construction practices or, in the best case, designed and realized based on surpassed criteria. This potential source of vulnerability to natural hazards becomes particularly relevant in regions prone to seismic events, such as those surrounding the Mediterranean basin, and rich in heritage assets. Among the others, past earthquakes that hit Italy

Stefania Degli Abbati and Daniele Sivori contributed equally to this work.

✉ Daniele Sivori
daniele.sivori@unige.it

Stefania Degli Abbati
stefania.degliabbati@unige.it

Serena Cattari
serena.cattari@unige.it

Sergio Lagomarsino
sergio.lagomarsino@unige.it

[1] DICCA, Department of Civil, Chemical and Environmental Engineering, University of Genoa, Via Montallegro 1, 16145 Genoa, Italy

have highlighted the huge cultural and economic losses following the damage and collapse of monumental structures such as fortresses [1, 2], palaces [3, 4], and churches [5–9], calling for effective seismic assessment procedures. These are necessary to identify the most critical cases and timely address the design and deployment of strengthening interventions (as widely discussed in [10–14]).

Indeed, the high degree of structural complexity and heterogeneity of historical structures—originating from the continuous transformations that occurred in their long-lasting life—affects the evaluation process detrimentally, being the source of uncertainties that can potentially propagate up to the assessment phase. An effective way to narrow down such uncertainties is the employment of dynamic testing, *i.e.*, the state-of-the-art nondestructive technique to experimentally investigate the dynamic behavior of existing structures (see [15] for a review of applications in Italy). Measurements of structural vibrations in operational conditions, known as ambient vibration tests (AVTs), are nowadays at the core of vibration-based continuous monitoring systems, being exploited to sense and diagnose the health conditions of monumental structures practically in real time [16].

In the historical built heritage, towers are among the most tested masonry structures by structural engineers, as shown by the richness of the literature on the subject. This trend can be reconducted not only to the need to preserve these old structures but also to the simplicity of the geometrical shape—dominated by the vertical dimension and several symmetries, which translates into quick experimental testing and straightforward modeling and analysis of the structural behavior. Measurements of environmental vibrations carried out on towers have been employed for dynamic investigations and structural identification purposes [17, 18] often addressed to the dynamic calibration of high-fidelity computational models [19–22], as well as to study the soil–structure interaction phenomena [23] or the efficacy of retrofitting interventions [24] and, more recently, for the continuous health monitoring and damage identification through permanent monitoring [25, 26].

Nonetheless, there are still relevant and challenging questions on the topic to be answered by the engineering research community. These issues are related to both practical aspects of experimental testing and continuous monitoring of masonry towers, such as sensing technology [27], sensors' optimal number and location, as well as to more advanced topics in data analysis and system identification, such as the removal of the effects of varying environmental conditions from the measured structural response [28]. Recently, huge efforts are being directed toward the real-time conjunction between experimental data and computational models—leading to the contemporary concept of digital twin (DT) of historical structures [29]. The interested reader can refer to [30] for a comprehensive review of the subject.

Alongside condition monitoring and damage assessment, a rising field of application is the employment of vibration measurements to improve the reliability of seismic evaluations on existing historical structures. This experimental approach is beneficial, even in the form of sporadic (or periodic) onsite testing, not only to evaluate a posteriori the effects of the earthquake on structures [31, 32] but also to enhance the initial knowledge phase [33], supporting the engineering judgement in defining the unknown modal and mechanical parameters to be employed in the formulation, calibration, and validation of analytical and computational models employed for the seismic assessment [34–37], ultimately improving its reliability.

In this context, the main purpose of the paper is to illustrate how the use of AVTs can improve the reliability of the seismic assessment of monumental structures, *i.e.*, the process of quantitatively assessing their seismic performance and identifying possible retrofit needs. To this aim, the manuscript presents the application to a case study, the bell tower of the Saint Lawrence Cathedral in Genoa, Italy, the most important medieval church of the city (Sect. 2). The structure is particularly interesting because of its monumental features and the fact of being partially embedded in the adjacent church, characteristics that make an accurate prediction of its seismic response a non-trivial task. In addition, the four pinnacles located on the upper terrace, due to their small size and high slenderness, were proven by past earthquakes to be architectonical elements significantly vulnerable to the seismic amplification caused by the tower.

An extended AVT campaign carried out on the structure allowed the identification of the dynamic behavior of the tower and the pinnacles, clarifying the underlying interaction with the main body of the church and its efficacy in constraining the tower's motion (Sect. 3). The assessment of the structure for the local seismic hazard is performed by analyzing both the global response of the tower (Sect. 4) and the local response of its artistic assets, *i.e.*, the pinnacles placed at its top (Sect. 5). The global seismic verification is obtained by relying on a simplified mechanical approach, which models the tower as a cantilever subjected to dead loads and horizontal forces caused by the earthquake and considers the possible activation of different collapse mechanisms—both shear and flexural behaviors. In addition, possible local mechanisms involving the out-of-plane response of the pinnacles are assessed by adopting a macro-block model and a displacement-based equilibrium analysis. Modal information provided by AVTs—in the form of operational natural frequencies and mode shapes—is employed, in the global verification of the bell tower, to accurately define the seismic forces acting on the tower and to quantify the constraint conditions imposed by the church. As a great point of novelty in the literature, the natural frequencies of the tower are employed to accurately estimate the seismic amplification in

height—in the form of floor spectra—to be used as the input forcing for the local verification of the pinnacles.

2 Brief historical notes and architectonic features of the Saint Lawrence Cathedral in Genoa, Italy

The Saint Lawrence Cathedral (Fig. 1a) is the most important church and probably the most majestic monumental structure in Genoa, Liguria Region, located in Northern Italy. According to the original project, which dates back to the medieval age, two bell towers placed at the opposite extremities of the façade were to be built. However, the left tower was never concluded and exists today as a "loggia" at the roof level.

The building of the right one, the actual bell tower of the church, (Fig. 1b) dates to the beginning of the XIV century and was concluded in 1522. The tower has a rectangular plan with sides of length about 10×12 m in the direction parallel (x-direction) and perpendicular (y-direction) to the façade, respectively. The total height reaches 73 m above the ground, at the top of the lantern. Two sides of the tower, the northeast and southeast, are contiguous to the church, the first to the main nave up to a height of around 27 m and the second to the lateral nave up to a height of around 20 m. While the external faces of the tower are characterized by a sequence of horizontal layers of white and black stone regularly superimposed onto each other, two different constructive phases can be identified for the internal structure of the walls. The lower part, from the ground up to the level from which the bell tower stands out from the church, is built with blocks of marly limestone stone arranged in a regular pattern over mortar layers. The upper part, conversely, is built with brick masonry with few limestone elements included. The bell tower ends with the presence of a bell chamber, a drum supporting a dome and, at the top, a lantern. Four soaring architectonic elements, the pinnacles, are located on the top terrace (Fig. 1b–c). All these elements show, quite systematically, a crack pattern of a certain severity (Fig. 1d), a probable consequence of the corrosion of internal steel elements fixing the cladding stone slabs to the masonry. Figure 1c–d shows, as an example, the crack pattern detected on the northeast pinnacle, the most severe among the ones recently surveyed.

The tower is built on five main levels connected by an internal spiral staircase running along the southeast corner. Masonry cross vaults compose the horizontal floor diaphragms—stone masonry for the lowest three and brick masonry for the others. The fifth level corresponds to the bell chamber and hosts a complex structure, built with timber beams and steel clamps supporting the iron bells. Different structural interventions involved the cathedral and its bell tower during their lifetime, including:

- in 1927, the vaults were unloaded of their filler and the southeast pillar of the bell tower was strengthened through the reinforcement of the spiral staircase, employing an internal reinforced concrete ("r.c." in the following) backbone.
- in 1929, a wall at the base of the tower was filled with r.c. to increase the structural stability of the cathedral. Some tie-rods were added on the façade, whereas the matroneum was reinforced with a base r.c. slab (Fig. 2a) and an r.c. arch (Fig. 2b);
- in 1933, a transversal wall running between the two towers was demolished (Fig. 2c).

Fig. 1 **a** General view of the Saint Lawrence Cathedral in Genoa; **b** east and north faces of the bell tower; **c** Northeast pinnacle on the top terrace; **d** detail of the crack pattern caused by the corrosion of anchoring steel elements

Fig. 2 Past structural interventions realized on the bell tower: (**a**, **b**). r.c. slabs and arch realized in 1929 in the matroneum; **c** demolition of the wall connecting the two towers in 1933

3 Identification of the bell tower dynamic behavior in operational conditions

3.1 Ambient vibration tests (AVTs) setup

To experimentally investigate the dynamic behavior of the Saint Lawrence bell tower in its operative conditions—*i.e.,* its vibrational response to ordinary but unmeasured excitation sources belonging to the environment—an extended AVTs campaign has been carried out on the structure in May 2020. Four independent acquisitions were performed in a time frame of a week, during which the local atmospheric conditions were quite stable in terms of temperature and humidity and characterized by a low-velocity wind. For these reasons, the influence of such factors on each daily test is neglected in the following analyses.

The layout of the accelerometer sensors has been properly conceived:

i. to determine the modal dynamics of the bell tower—*i.e.*, frequencies and mode shapes of the fundamental and higher modes of vibration along each main direction of the tower—and, similarly, of the non-structural elements placed at the top (the pinnacles);
ii. to study the dynamic interaction with the main body of the church, in particular with the main facade and matroneum along the NS direction, and with the south aisle along the EO direction.

For what concerns the global seismic assessment of the bell tower, this strategy has the double purpose of calibrating the modal properties and the boundary conditions of the simplified mechanical model employed for the verification (Sect. 4). Sensors localized on the top terrace and the pinnacles allow, in the complementary seismic assessment of non-structural elements, an accurate estimation of amplification effects, as well as the possible rise of resonance phenomena between the main structure and the secondary elements (Sect. 5).

The sensor layout is schematically reported in Table 1. The experimental setup consists of four independent measurement configurations (referred to as "CNF"), which differ in the positioning of the sensors but always share at least one or more reference sensors in a fixed position. For each sensor, letters indicate positions in the plan, whereas numbers refer to the corresponding level along the height. Configurations CNF1, CNF2 (and partly CNF4) extend on the bell tower in all its accessible levels—level L1: matroneum, level L2: "seminaristi" room, level L3: deposit room, level L4: bell chamber, level L5: top terrace—with at least two horizontal bi-axial sensors placed at the opposite corner of each floor (Fig. 3). Moreover, one bi-axial sensor is placed at the top of each pinnacle shaft (level L5*). Configurations CNF3 and CNF4 mainly involve the body of the church (Fig. 4), in particular, the matroneum and north "loggia", the main nave (level L2) and south nave (level L1*). In the general case, sensors are

Table 1 AVTs sensor layout for each measurement configuration deployed, both for the bell tower and the church

Configuration	Bell tower		Church		Reference
	Area of interest	Position	Area of interest	Position	
CNF1	Pinnacles, terrace, bell chamber	A5*–B5*, C5*–D5*, A5–C5, A4–C4	//	//	//
CNF2	Deposit, "seminaristi" room	A3–C3, A2–C2	//	//	A5–C5
CNF3	//	//	Façade and "loggia", main nave and south nave	E2–G2, F2–K2, H1*	A5–C5
CNF4	Matroneum	A1–C1	Façade and matroneum	E1–G1	C5

integral to the structure by gravity (see, for example, positions A4–C4 in Fig. 3). In the case of reference positions, a metal bracket holding the sensor is mechanically fixed to the masonry through bolts (positions A5–C5 in Fig. 3).

3.2 Data processing and dynamic identification

The environmental response of the structure has been measured, for each configuration, from a single acquisition lasting between 35 min (CNF3 and CNF4) and 45 min (CNF1 and CNF2, shown in Fig. 5) with a sampling frequency of 200 Hz. The sensors, made by *Geospace* and assembled by the Italian *Solgeo*, are high-sensitivity velocimeters suited to accurately measure low-amplitude and low-frequency oscillations. Each sensor houses three geophones mounted orthogonally and electronically linearized to an eigenperiod of 1 s, providing a measurement frequency range extending from 1 Hz up to 315 Hz and ensuring a flat frequency response between 1 and 64 Hz. The sensing elements are characterized by a sensitivity of 400 V/m/s, a spectral noise of 55 nm/s (RMS 1–315 Hz), and a dynamic range exceeding 130 dB. The signals are digitalized by a six-channel proprietary acquisition system, which is equipped with an individual 24-bit AD converter for each channel and a digital anti-aliasing filter, providing a dynamic range of 130 dB at 100 Hz. Each system is synchronized with the absolute time via an independent GNSS receiver. The velocity signals are initially pre-processed (decimation, low-pass filtering) to facilitate their subsequent elaboration. Dynamic identification is performed with a well-known technique belonging to the frequency domain, the so-called frequency domain decomposition (FDD, [38]). The identification involves the singular value decomposition of the cross-spectral density matrix of the signals. More in detail, the power spectral densities (PSD) were estimated by employing the well-known Welch method, fixing the frequency resolution to 0.01 Hz.

The natural frequencies of the structure are identified—assuming the corresponding modes to be well separated in frequency—at the peaks of the first singular value (Fig. 5), whereas the mode shapes are extracted from the corresponding singular vector. A phase check (modal phase collinearity index, MPC [39]) allows a robust picking of the spectral amplification bells originating from structural modes. In particular, possible spurious modes related to unknown harmonic inputs are ruled out according to the lack of phase collinearity (lower bound MPC fixed to 0.8). Finally, the natural frequencies f_n and quality indices MPCs of the system are estimated as the average value of those identified in each configuration, the global mode shapes are reconstructed based on the amplitude response of the reference sensor(s). Modal displacements from different measurement configurations have been first scaled to unitary amplitude at the reference sensor and then merged. A least-squares approach was adopted when two reference sensors were available (CNF2 and CNF3).

A total of nine structural modes with high phase collinearity are identified in the range between 1 Hz and 5.5 Hz (Table 2). The first two experimental modes involve the flexural behavior of the tower along its principal axes—mode B-G-Fx at 1.57 Hz in direction x and mode B-G-Fy at 2.03 Hz in direction y, Fig. 6—and exhibit the maximum spectral amplification, approximately two orders of magnitude greater than the one exhibited by higher frequency modes. Several amplification peaks, identifiable in the frequency range between 2.99 Hz and 5.5 Hz, correspond to modes of the church involving globally its main body or, locally, the matroneum/façade, as well as to higher modes of the bell tower (torsional and higher order flexural modes). It should be noted how, in general, the church and the bell tower appear to be strongly coupled, so that the two structures participate with relevant

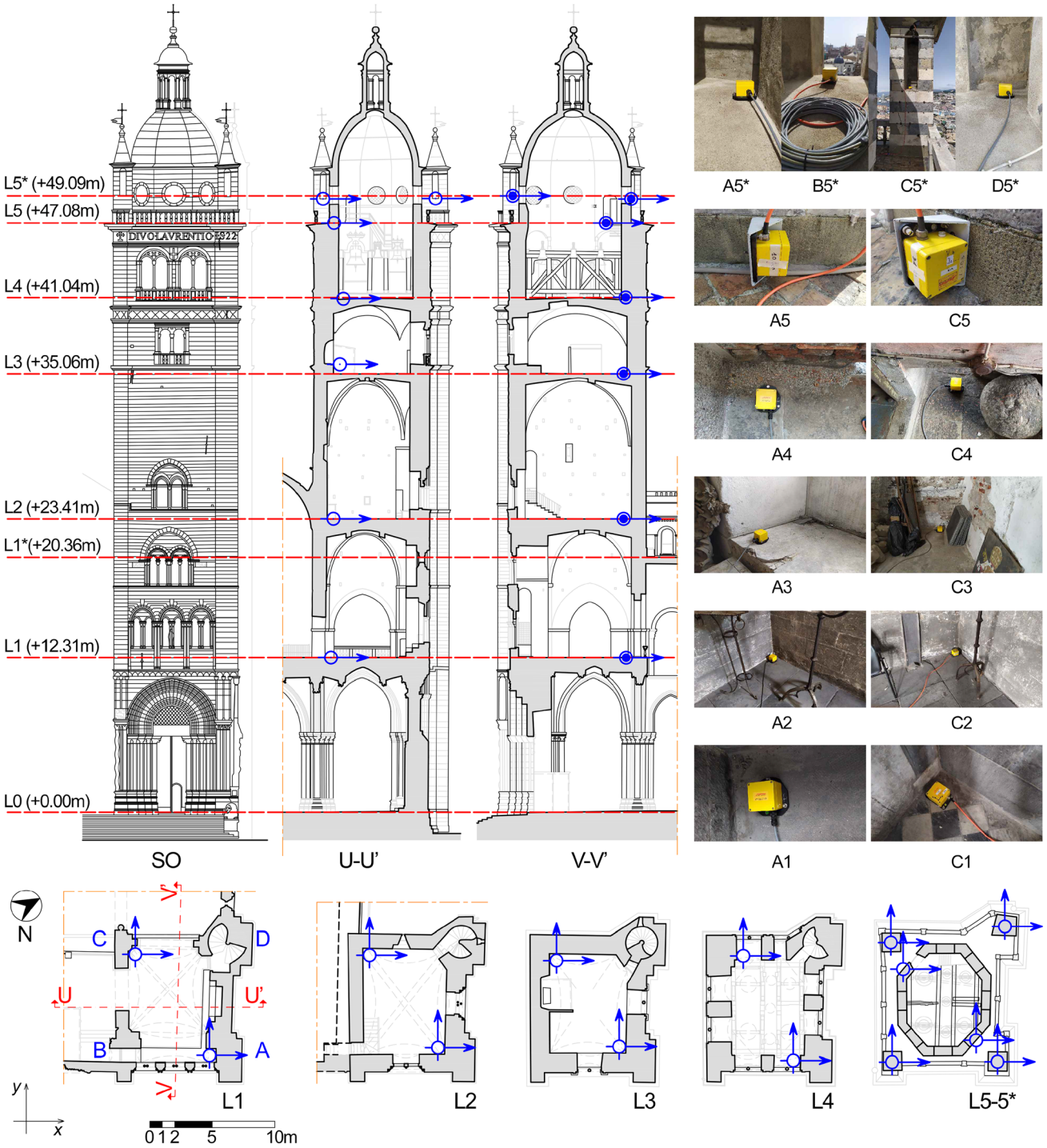

Fig. 3 AVT sensor layout for the bell tower (measurement configurations CNF1 and CNF2 plus A1–C1)

modal displacements in most of the identified modes. This is particularly true for the torsional modes—in which the church and the bell tower interact with the same phase—and for second-order flexural modes of the bell tower—in which the body of the church moves in opposition of phase with respect to the top of the tower (Fig. 6). Several peaks in the frequency range between 5.5 Hz and 9 Hz, as highlighted by the level of spectral amplification of the corresponding measurement channels (dash-dotted lines in Fig. 5, CNF1), can be reconducted to the modes of vibration of the pinnacles.

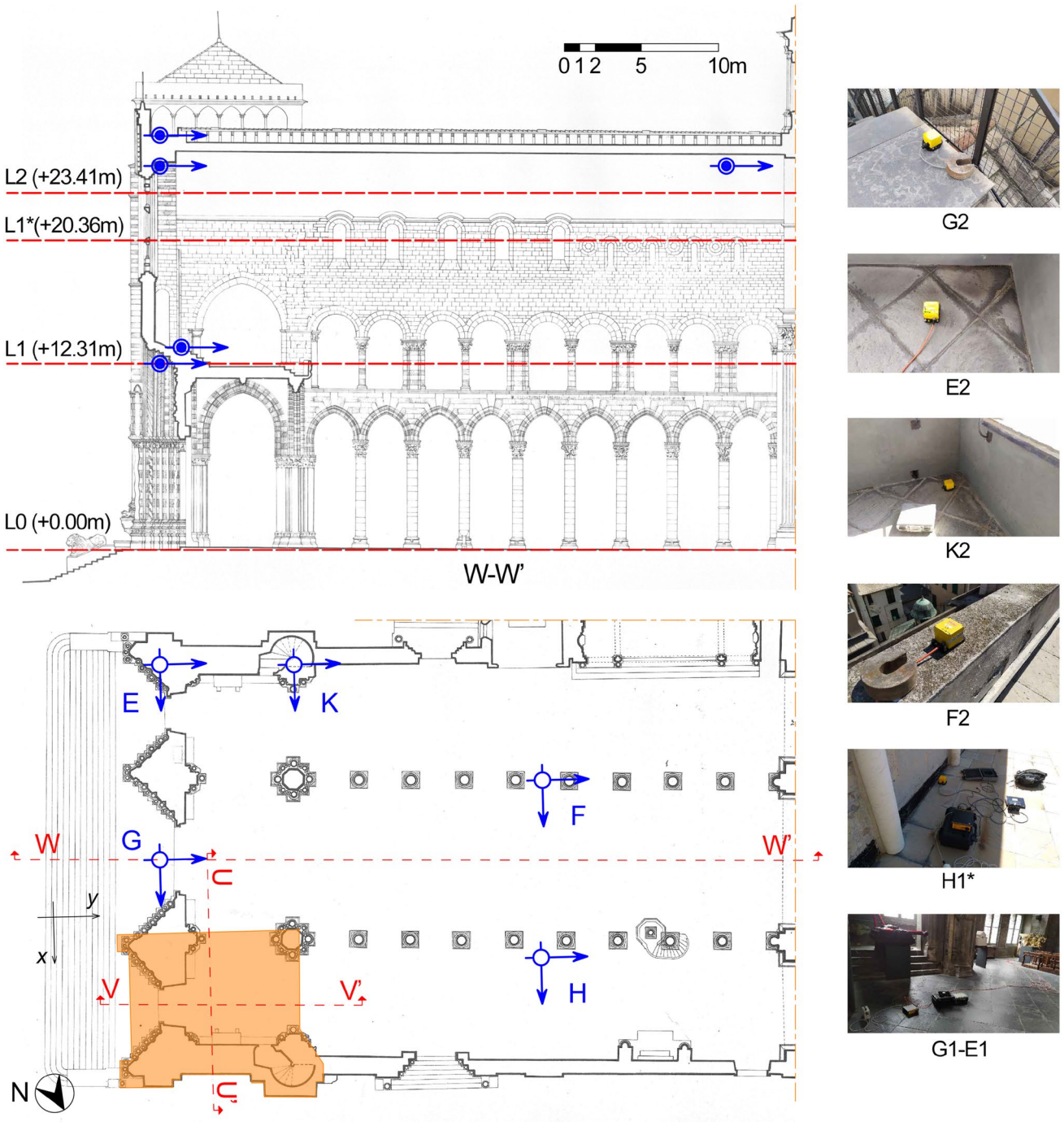

Fig. 4 AVT sensor layout for the church (measurement configurations CNF3 and CNF4)

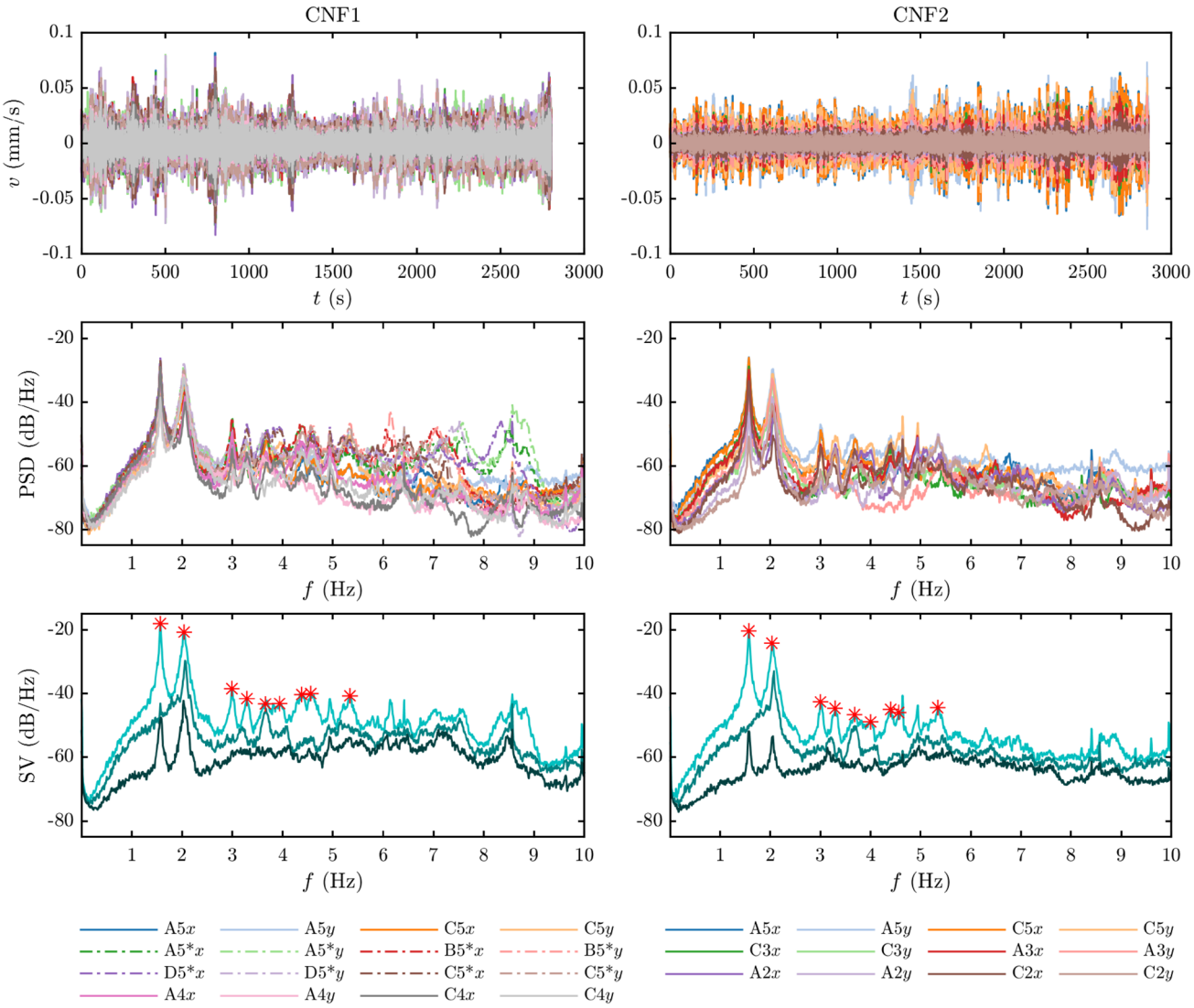

Fig. 5 Measurement configurations CNF1 and CNF2. Ambient vibrations time history (velocity v in mm/s), power spectral density (PSD) and first three singular values (SV), highlighting ten amplification peaks identified as structural modes

Table 2 Structural modes characterizing the bell tower, the church, and their dynamic interaction. The modes result from the merging of four independent AV single acquisitions (performed in the time frame of a week in May 2020)

Mode	Name	Part	Type	Description	f_n (Hz)	MPC
1	B-G-Fx	Bell tower	Global	First-order flexural mode along x	1.57	0.98
2	B-G-Fy	Bell tower	Global	First-order flexural mode along y	2.03	0.97
3	C-G-Tx	Church	Global	Translational mode along x	2.99	0.92
4	L-Ty	Matroneum	Local	Translational mode along y	3.28	0.90
5	C-G-Ty	Church	Global	Translational mode along y	3.65	0.87
	B-G-Fx2	Bell tower	Global	Second-order flexural mode along x		
6	C-G-Tx2	Church	Global	Translational mode along x	3.96	0.81
7	B-G-Rz	Bell tower	Global	Torsional mode around z	4.36	0.85
8	C-G-Rz	Church	Global	Torsional mode around z	4.55	0.82
	B-G-Rz	Bell tower	Global	Torsional mode around z		
9	B-G-Fy2	Bell tower	Global	Second-order flexural mode along y	5.33	0.83
	P-L	Pinnacles	Local	First-order flexural modes	5.5–9	//

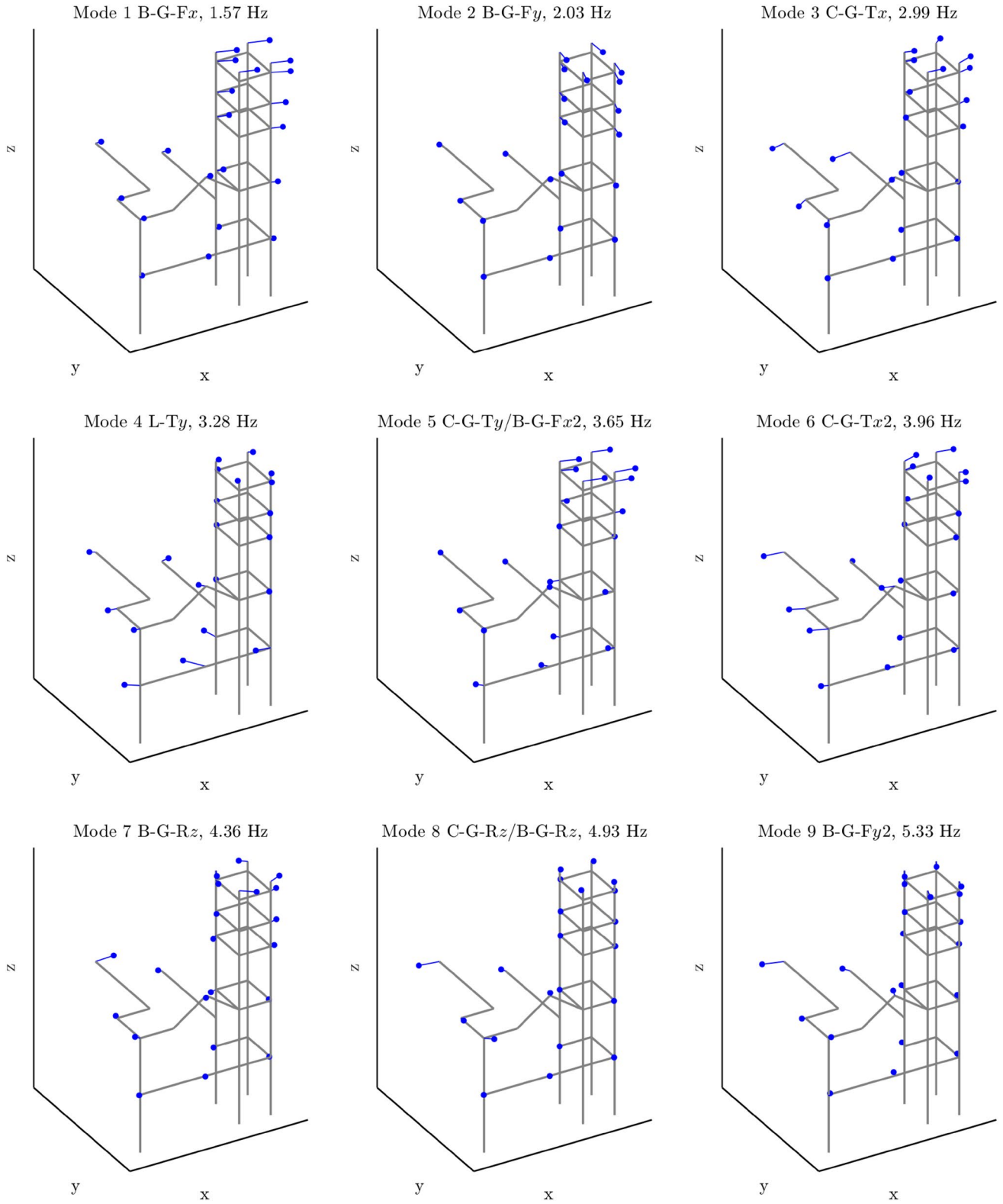

Fig. 6 Experimental mode shapes resulting from the merging of multiple measurement configurations (see the description of each setup and the relative reference sensor in Table 1).

4 Global seismic assessment of the bell tower

4.1 Definition of the analysis model and assumed mechanical parameters

The global seismic assessment of the bell tower has been performed with the software DBV-Tower, a MATLAB implementation of the analytical model proposed in [40]. This approach derives from the simplified mechanical model proposed in the Italian guidelines for the evaluation and mitigation of the seismic risk for the cultural heritage [41], which models the tower as a cantilever subjected to dead loads and a system of horizontal forces, those generated by the earthquake.

According to the simplified modeling strategy first introduced in [41], the verification is carried out at different levels of the structure according to their cross-sectional properties, considering a combined collapse mechanism due to compressive and bending stresses under the assumptions of (i) conservation of flat sections, (ii) nontensile resistant masonry, (iii) rectangular stress-block diagram for compression. Extending the capabilities of this approach, the application presented in this paper considers the further possibility to account for the shear failure, as introduced in [40]. This choice follows the observation of damage on towers after the 2012 Emilian earthquake, which clearly showed that the combined compressive and bending failure was not the only possible damage mechanism [1, 2]. Furthermore, in [40], the assumed mode shape derived from a simplified empirical formula that requires an appropriate calibration, especially if annexed structures—in the case examined, the church—could influence the dynamic behavior of the tower. For this reason, as an original contribution of the article, the mode shapes of the fundamental modes experimentally identified from AVTs for each direction (see Sect. 3.2) are employed in place of the simplified expressions reproducing the constraint conditions of the adjacent church, improving the reliability of the model adopted for the verification.

The main steps of the assessment procedure are applied to the case study in the following. The interested reader can refer to [40] for further details regarding the original approach.

The simplified mechanical model requires the tower to be divided, along its height, into sectors with homogeneous geometrical and mechanical features, accounting for possible variations in the resistant area as well as in the seismic capacity

Table 3 Geometrical, material, and mechanical properties of each sector considered for the bell tower

Sector i	z_i (m)	h_i (m)	A_i (m^2)	γ (kN/m3)	V_i (m^3)	W_i (kN)
1	3.22	6.44	43.98	22	283.23	6231
2	8.26	3.64	46.30		168.52	3708
3	11.195	2.23	65.40		145.84	4021
4	12.68	0.74	30.68		22.70	499
5	14.305	2.51	20.89		52.43	1153
6	16.795	2.47	32.40		80.02	1760
7	18.985	1.91	36.93		70.53	1552
8	21.675	3.47	38.08		132.13	3836
9	23.79	0.76	48.70		37.01	814
10	25.07	1.80	42.51		76.52	1683
11	27.185	2.43	47.58		115.62	2544
12	31.72	6.64	48.01		318.79	8070
13	35.395	0.71	55.56	18	39.44	710
14	36.145	0.79	55.30		43.69	786
15	37.555	2.03	49.51		100.50	1809
16	39.8	2.46	55.56		136.67	3403
17	41.415	0.77	58.33		44.91	808
18	43.13	2.66	32.04		85.22	1534
19	45.41	1.90	58.33		110.82	1995
20	46.72	0.72	68.90		49.60	893
21	47.89	1.62	21.38		34.63	623
22	48.985	0.57	13.60		7.75	140
23	49.68	0.82	14.37		11.78	212
24	50.86	1.54	22.15		34.11	1622

h height, A cross-sectional resistant area, γ specific weight, V volume, W total weight

of the cross-section. Among the others, these differences are determined by the presence of openings, the reductions in the thickness of masonry walls, sudden changes of materials and/or different construction phases, the presence of intermediate horizontal diaphragms, and the influence of adjacent structures at the boundaries. Table 3 reports, for each i-th sector among the N considered ($i=1, \ldots, N$ with $N=24$), the geometrical properties and the resistant area of the walls A_i.

The verification is carried out according to the two principal inertia directions of the tower x and y. Being not possible to identify a priori the most critical one, all the sectors were considered in the analysis. In particular, an equivalent distribution of static forces is defined as a function of the identified modal shape $\Psi(z_i)$, then the force applied to each sector F_i is computed according to Eq. (1) and, last, the generalized internal forces—the shear V_i and the moment M_i—are calculated at each level according to Eqs. (2) and (3), where W_i is the sector weight, h_i is the sector height, z_i and z_k are the heights of the centroid of sectors i and k with respect to the ground. F_{1i}, $v_{1,i,}$ and $m_{1,i}$ in Eqs. (1), (2), and (3) are multiplicative coefficients of the total seismic base shear F_b (they collect the entities included in brackets).

$$F_i = F_b\left(\frac{W_i\psi(z_i)}{\sum_{k=1}^{n} W_k\psi(z_k)}\right) = F_b F_{1i} \tag{1}$$

$$V_i = F_b\left(\frac{\sum_{j=i}^{n} W_j\psi(z_j)}{\sum_{k=i}^{n} W_k\psi(z_k)}\right) = F_b v_{1i} \tag{2}$$

$$\begin{aligned} M_i &= F_b\sum_{j=i}^{n} F_j\left(z_j - z_i + \frac{h_i}{2}\right) = F_b\left(\frac{1}{\sum_{k=i}^{n} W_k\psi(z_k)}\right) \\ &\times\left[\sum_{j=i}^{n}\left(W_j\psi(z_j)z_j\right) + \left(z_i - \frac{h_i}{2}\right)\sum_{j=i}^{n} W_j\psi(z_j)\right] = F_b m_{1i} \end{aligned} \tag{3}$$

The ultimate shear $V_{u,i}$ and the ultimate moment $M_{u,i}$ are estimated according to Eqs. (4) and (5), by additionally introducing the strength properties of the masonry. In particular: a_i and b_i are the two orthogonal dimensions of sector i; $b_{0,i}$ is the length of the opening(s) on side b (if present); t_i is the wall thickness; f_m is masonry compressive strength; $\sigma_{0,i}$ is the compressive stress state; $V_{0u,i}$ is the ultimate shear strength.

$$M_{u,i} = 0.5\sigma_{0,i}A_i b_i\left(1 - \frac{\sigma_{0,i}A_i}{0.85 f_m a_i b_i}\right) \tag{4}$$

$$V_{u,i} = V_{0u,i}\left(1 - \frac{b_{0,i}}{b_i - 2t_i}\right)\frac{b_i - b_{0,i} - 2t_i}{\sqrt{\frac{4}{3}h_i^2 + \left(b_i - b_{0,i} - 2t_i\right)^2}} \tag{5}$$

The shear strength $V_{0u,i}$ can be computed according to common criteria proposed in the literature, by choosing the most appropriate for the observed masonry typology (as discussed in [42], such as the proposal of Turnsek and Cacovic [43] for the case of irregular masonry, or that of Mann and Muller [44] for a more regular one). In such a way, the strength properties affecting the shear failure modes (*i.e.*, the equivalent tensile shear strength, in the case of [43], the cohesion, the friction coefficient and the interlocking parameter, in the case of [44]) explicitly come into play. The ultimate moment $M_{u,i}$ is evaluated based on the beam theory, neglecting the tensile strength of the material and matching the failure with the attainment of the compressive strength of masonry at the compressed toe. Both the criteria require the evaluation of the vertical stress $\sigma_{0,i}$ acting on each sector, as generated by the weight of the sectors above and the dead loads of the floors.

Finally, the ultimate strength of the tower is obtained in terms of total seismic base shear F_b according to Eq. (6), where $v_{1,i}$ and $m_{1,i}$ are nondimensional coefficients already introduced and defined in Eqs. (2) and (3), respectively. In this way, it is possible to identify the weakest section and

Table 5 Area loads associated with each vault of the tower

Horizontal diaphragm typology	q (kN/m^2)
Stone masonry cross vault—level L1	21*
Stone masonry cross vault—level L2	22
Stone masonry cross vault—level L3	15
Brick masonry cross vault—level L4	15
Dome	27

*An additional load equal to 0.6 kN/m^2 is considered due to a 3-cm-thick reinforced concrete slab, realized on this vault during the interventions of the 1930s

Table 4 Mechanical parameters assumed for the masonry typologies surveyed on the bell tower

Masonry typology	Classification [45]	f_m (N/mm^2)	τ_0 (N/mm^2)	γ (kN/m^3)
Blocks of marly limestone arranged in regular layers	Squared stone blocks	7	0.105	22
Brick masonry with few marly limestone elements	Brick masonry with lime mortar	3.45	0.09	18

the corresponding collapse mechanism (shear or combined bending–compression).

$$F_{b,i} = min\left\{\frac{V_{u,i}}{v_{1,i}}; \frac{M_{u,i}}{m_{1,i}}\right\} \quad (6)$$

Table 4 collects the material and mechanical parameters assumed in the analysis. The strength properties correspond to the average values of the range proposed by the Italian Technical Code [45] for each masonry typology characterizing the bell tower, namely, limestone blocks arranged in regular layers, in the lower part, and brick masonry, in the upper part. In this application, the estimation of $V_{0u,i}$ follows the criterion proposed by [43]. Table 5 summarizes the gravitational loads associated with the vaults at different levels, obtained from the available geometrical data and assuming specific weights of 22 kN/m^3 for stone masonry vaults, 18 kN/m^3 for brick vaults and the dome, 13 kN/m^3 for the vault filler.

A crucial aspect to be accounted for, to accurately reproduce the dynamic behavior of bell towers when subjected to seismic actions, is the effectiveness of the constraint offered by the adjacent church or by other interacting bodies, when they are present. In this paper, the issue is addressed by employing the results of AVTs (Sect. 3), which allowed to identify the actual deformed shape of the tower (Sect. 3.2). More specifically, the fundamental flexural modes of the bell tower—mode B-G-F*x* and mode B-G-F*y*— were considered to be governing the seismic response of the tower along each main direction.

To deepen the matter, it is of great interest to compare the fundamental elastic period of the system T_1 identified experimentally for each main direction, $T_1 = 0.638$ s along *x* and $T_1 = 0.493$ s along *y* (corresponding to mode B-G-F*x* and mode B-G-F*y*, Table 2), to the one obtainable applying the empirical formula $T_1 = 0.0187H$ proposed by technical codes, where H is the free height of the tower.

The formulation has been alternatively applied considering the tower:

(a) to be isolated, completely neglecting the interaction with the adjacent church and assuming a free height H of about 50 m (up to the drum supporting the dome);
(b) to be effectively constrained by the adjacent church, thus assuming a free height H of about 28 m.

The two assumptions, isolated and restrained, lead to $T_1 = 0.94$ s and $T_1 = 0.52$ s, respectively. As expected, the experimental and analytical periods are much closer when assuming the tower to be restrained by the church, whereas the analytical period for the isolated-tower case is significantly higher than the one identified from ambient vibration measurements. Such a comparison confirms the effectiveness of the constraint offered by the church, as previously suggested by experimental data (Sect. 3.2), quantifying how this boundary condition strongly affects the natural periods and the mode shapes of the tower.

Indeed, it is well known that the dynamic properties of structures undergoing high-amplitude seismic vibrations may differ significantly from those identified under operational conditions, in the low-amplitude vibration regime. These variations are usually more relevant for frequencies and damping ratios than for mode shapes. Generally, an increase in the vibration amplitude leads to a transient decrease in the (instantaneous) natural frequency, *i.e.*, to an elongation of the elastic natural period, which is observed in the co-seismic phase even in the absence of structural damage. In reinforced concrete structures, these effects are usually linked to the interaction between structural and non-structural elements [46, 47]. In masonry structures, the temporary opening of pre-existing cracks [48] and the deterioration of the wall-to-wall and wall-to-diaphragm connections may play a more important role. In the tower analyzed, these effects are plausibly limited by the good quality of the masonry and by the continuity between the church and the tower walls, factors which ensure effective connections between vertical and horizontal resistant elements. These reasons justify the assumption of operational dynamic properties, natural period, and mode shapes, as representative indicators of the dynamic response to earthquake actions in the global seismic verification of the structure (Sect. 4.2), at least in the first phase of the response.

4.2 Results of the global seismic assessment

The seismic assessment of the bell tower has been carried out according to the limit state (LS) of life-safety, hereinafter named "SLV", based on a linear static approach. The seismic input has been defined according to the Italian Technical Code [49] by adopting a return period T_R equal to 712 years, which corresponds to a reference life V_R equal to 75 years (considering a nominal life $V_N = 50$ years and a class of use III, "buildings with a significant crowd", which corresponds to a use coefficient $C_U = 1.5$) and a probability of exceedance of the seismic action equal to 10% in V_R. A soil of type B has been assumed, as reasonably deduced from the available historical notes. Table 6 collects the seismic parameters defining the seismic response spectrum in Genoa: a_g is the peak ground

Table 6 Parameters defining the seismic response spectrum for SLV (life-safety) at the site

T_R (years)	a_g (g)	S	$S_{a,g}$ (g)	F_0	T_B (s)	T_C (s)	T_D (s)
712	0.079	1.2	0.0948	2.534	0.137	0.412	1.914

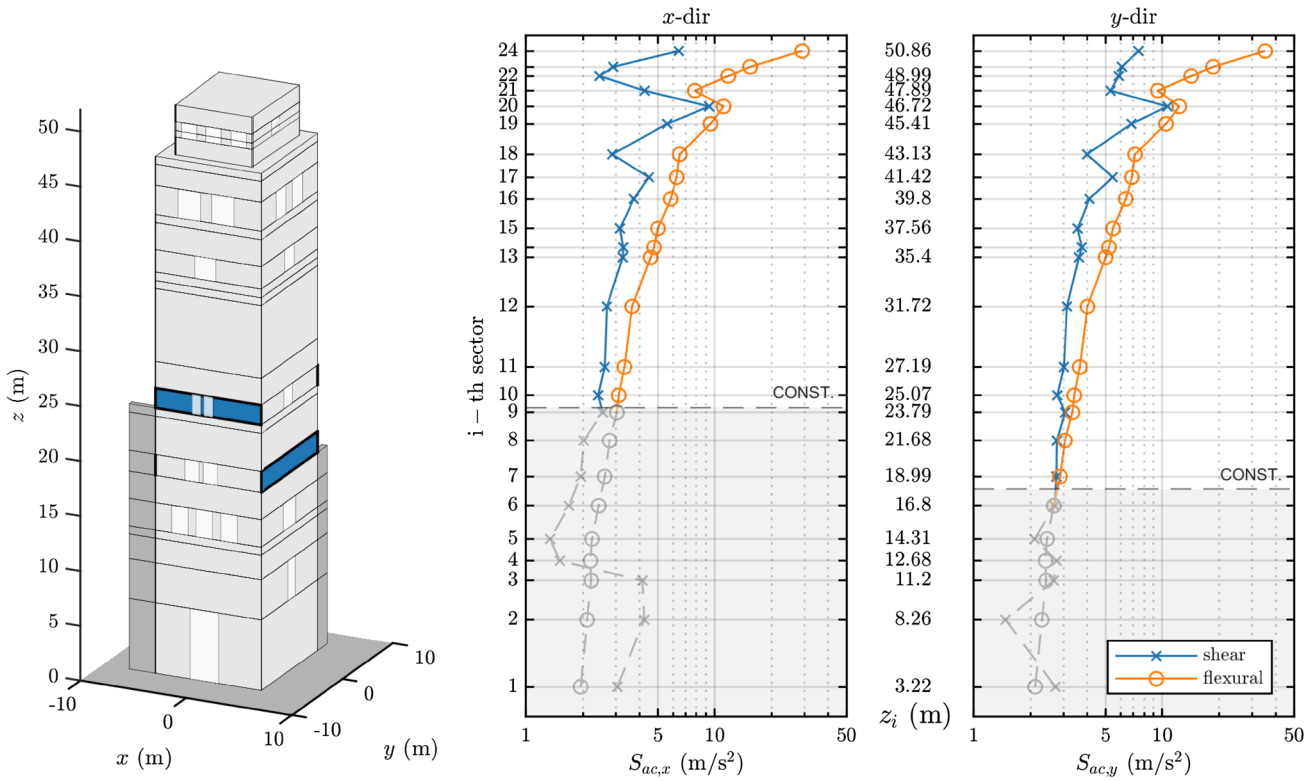

Fig. 7 Spectral acceleration profiles leading to the shear and flexural failure of each sector of the bell tower, for x and y directions

horizontal acceleration on rocky soil; S is the soil factor to account for the topographic and stratigraphic effects; $S_{a,g}=a_g S$ is the peak ground acceleration at the site; F_0 is the maximum amplification factor of the horizontal acceleration spectrum; T_B, T_C, and T_D are the periods characterizing the different branches of the response spectrum.

To compare the resistance of the tower to the seismic demand at the site, the forces achieving the resistance of each sector are expressed in terms of seismic accelerations through Eq. (7). The maximum-allowed demand $S_{a,\max}$ defined in Eq. (8) corresponds, thus, to the failure of the sector characterized by the minimum global resistance, independently of the activated failure mechanism.

$$S_{ac,i} = F_{b,i} g \frac{\sum_{k=1}^{n} W_k \psi(z_k)^2}{\left[\sum_{k=1}^{n} W_k \psi(z_k)\right]^2} \tag{7}$$

$$S_{a,max} = min\{S_{ac,i}\} \tag{8}$$

Figure 7 shows the trend of the spectral accelerations corresponding to the achievement of the SLV state for each of the considered sectors. The profiles represent the failure scenario expected during the earthquake, as provided by the minimum between the two possible collapse mechanisms—shear and flexural. The horizontal dashed line indicates the detachment height of the tower. Under this level, the actions induced on the bell tower are partially transferred to the church walls (facade and south nave), which are assumed to provide an effective constraint in both verses for the considered mechanisms. It can be observed that, above the detachment height, the activation of a shear mechanism is expected in both directions, since the shear resistance is always lower than the flexural one. However, along the y-direction, the two mechanisms exhibit similar activating accelerations for the first sectors above the detachment height, whereas the acceleration profiles leading to the shear and flexural failure in the x-direction are much different. In both cases, the minimum resistance, *i.e.*, the maximum-allowed demand, corresponds to the failure of the first sector above the constraint provided by the church, sector 10 and

Table 7 Results of the global seismic assessment of the bell tower at SLV in terms of safety index I_s

$T_{1,x}$ (s)	$T_{1,y}$ (s)	$S_a(T_{1,x})$ (m/s²)	$S_a(T_{1,y})$ (m/s²)	$S_{a,\max,x}$ (m/s²)	$S_{a,\max,y}$ (m/s²)	$I_{s,x}=PGA_{C,x}/PGA_{D,x}$	$I_{s,y}=PGA_{C,y}/PGA_{D,y}$
0.638	0.493	1.521	1.982	2.409	2.743	1.58	1.38

sector 7 for the *x*- and *y*-direction, respectively. It is interesting to compare these results with those obtained considering the bell tower as isolated, *i.e.*, neglecting the restraining effect and the masses provided by the church. The grey profiles below the constraint in Fig. 7, representative of the actions induced on the bell tower ideally isolated, indicate that the failure mechanism would instead occur in the lower sections of the tower—those characterized by mullioned windows. This outcome further highlights the primary role played by the church in determining the bell tower response (see Sect. 4.1).

Table 7 summarizes the results of the global seismic assessment of the bell tower. In particular, the acceleration demand calculated as the spectral acceleration corresponding to the fundamental period $S_a(T_1)$ is compared to the maximum-allowed spectral acceleration $S_{a,\max}$—the minimum value above the detachment height. T_1 corresponds, for each direction, to the period experimentally identified (see Sect. 3.2) for the fundamental flexural modes of the tower, mode B-G-F*x* for the *x*-direction and mode B-G-F*y* for the *y*-direction, as defined in Sect. 4.1. This indeed corresponds to the verification with respect to the elastic limit. The result of such a comparison is exemplified by the safety index I_s, computed with respect to the peak ground acceleration PGA as the ratio between capacity (PGA_C) and demand (PGA_D). It has to be specified that a constant spectral shape has been assumed with reference to the parameters summarized in Table 6, once verified from the hazard map that their variation is almost negligible in the range of the interested return periods.

The results show that the most vulnerable direction is *y*, which is associated with the lowest value of the safety index. However, the verification is always satisfied, being the safety index I_s higher than one for both directions. The results confirm the good structural quality of the monument and, considering that the expected seismic hazard in Genoa is not so relevant, appear fully justified.

It is worth highlighting that, in the estimation, the effect of the behavior factor has been neglected, even though its use would be justifiable by considering that the verification refers to the SLV. In this sense, the safety indexes of Table 7 have to be intended as precautionary. The adoption of a reference behavior factor specific to the bell tower would be quite conventional, since the values proposed in national codes (see [45, 49]) have been developed and validated for other structural typologies, mostly residential buildings [50], and no specific studies on towers are available in the literature.

The assessment refers, in such a case, to the strength capacity of the system. More in general, the method proposed in [40] allows proceeding further with a displacement-based approach, building the capacity curve of the system. This development was judged not necessary for this case study, given the positive outcome already achieved from the linear static approach.

5 Local seismic assessment of the pinnacles

5.1 Assessment procedure through a macro-block model

To achieve a comprehensive seismic assessment of the bell tower as a whole, the non-structural elements located at the top, the pinnacles, have been verified against the activation of potential mechanisms in the form of rigid block motions. To assess the pinnacles' ultimate behavior, nonlinear kinematic analyses adopting a macro-block model (MBM) approach are carried out by exploiting the MB-Perpetuate

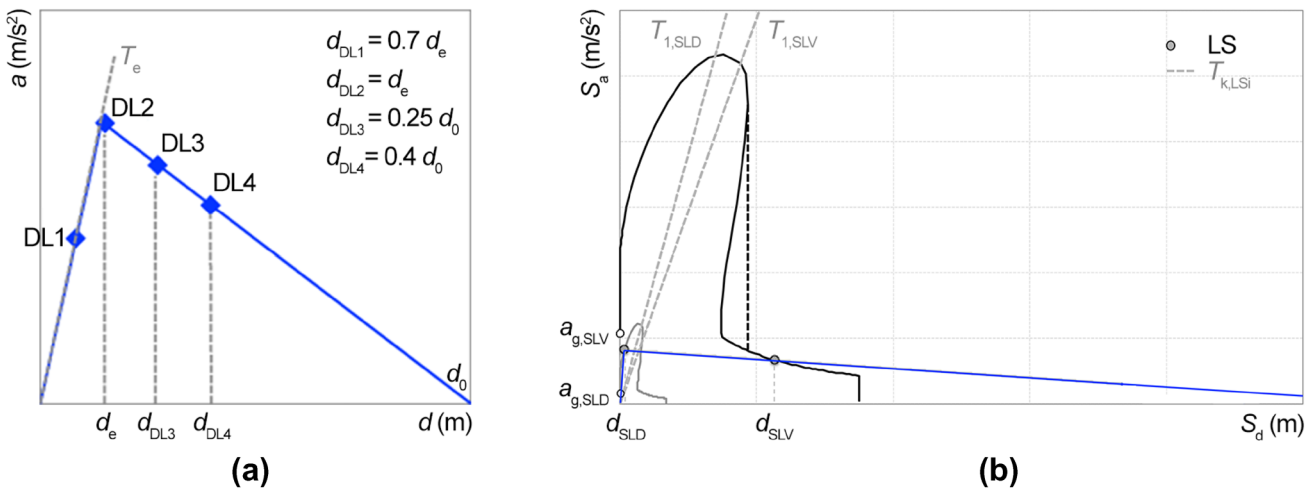

Fig. 8 Out-of-plane seismic assessment of pinnacles. **a** Definition of the bi-linear capacity model and identification of DL thresholds; **b** intersection between the capacity curve of the system and scaled floor spectra to assess the peak ground acceleration a_g associated with each LSs

code [51], a software developed in the framework of the Perpetuate Project [52].

The seismic assessment is based on the displacement-based approach illustrated in [53], whose reliability has been validated in [54] through the comparison of results achieved from nonlinear dynamic analyses. The method allows building a capacity curve of the system, as well as the identification of LS displacement thresholds and the definition of the criteria providing the seismic demand—criteria coherent with the ones prescribed in [45]. Regarding the first aspect, Fig. 8a shows the bi-linear capacity curve assumed for the pinnacles, on which damage levels (DLs) are first identified and then associated with the corresponding LSs. It is possible to observe how such a curve differs from the ideal one characterizing the loss of equilibrium of a rigid body for overturning. The assumed bi-linear behavior—characterized by a first elastic branch with an initial elastic period T_e— is, in this respect, closer to the one exhibited by real structures [55].

The seismic assessment has been performed by associating DL4 with the life-safety limit state (SLV). This limit state is defined by the displacement $d_{SLV} = 0.4d_0$, where d_0 corresponds to the load multiplier reaching zero under static conditions (i.e., to the collapse for overturning). The capacity curve of the system is then compared with the seismic demand, represented through a response spectrum (Fig. 8b). Since the local mechanisms under verification involve macroelements placed at the top of the tower, a floor response spectrum must be considered to reliably account for the filtering effect provided by the main structure [56–60]. For such a purpose, in this paper, the floor response spectrum was calculated according to the practice-oriented expression proposed in [45]. The expression is based on the analytical formulation originally proposed by some of the authors in 2018 [61] and recently validated using response measurements acquired on monitored structures during the 2016/2017 Central Italy earthquake [62]. Considering that the bell tower amplifies the induced motions at the base of the pinnacles and this phenomenon mostly depends on its dynamic properties, the modal parameters identified in Sect. 3.2 are employed to accurately evaluate the floor response spectrum to be used as seismic input in the verification of the pinnacles. More details regarding the application to the case study under investigation are provided in Sect. 5.2.

The final step of the local assessment involves the comparison between the capacity curve of the system and the floor spectrum demand. According to [45], the spectrum has been "smoothed" to associate monotonically increasing displacements to increasing periods in the spectral displacement–acceleration plane (dashed spectrum in Fig. 8b). The intersection between capacity and scaled demand allows estimating the peak ground acceleration a_g (selected as the intensity measure IM of the input) necessary to achieve each considered LS.

For what concerns the assumed MBM, two kinds of mechanisms have been analyzed:

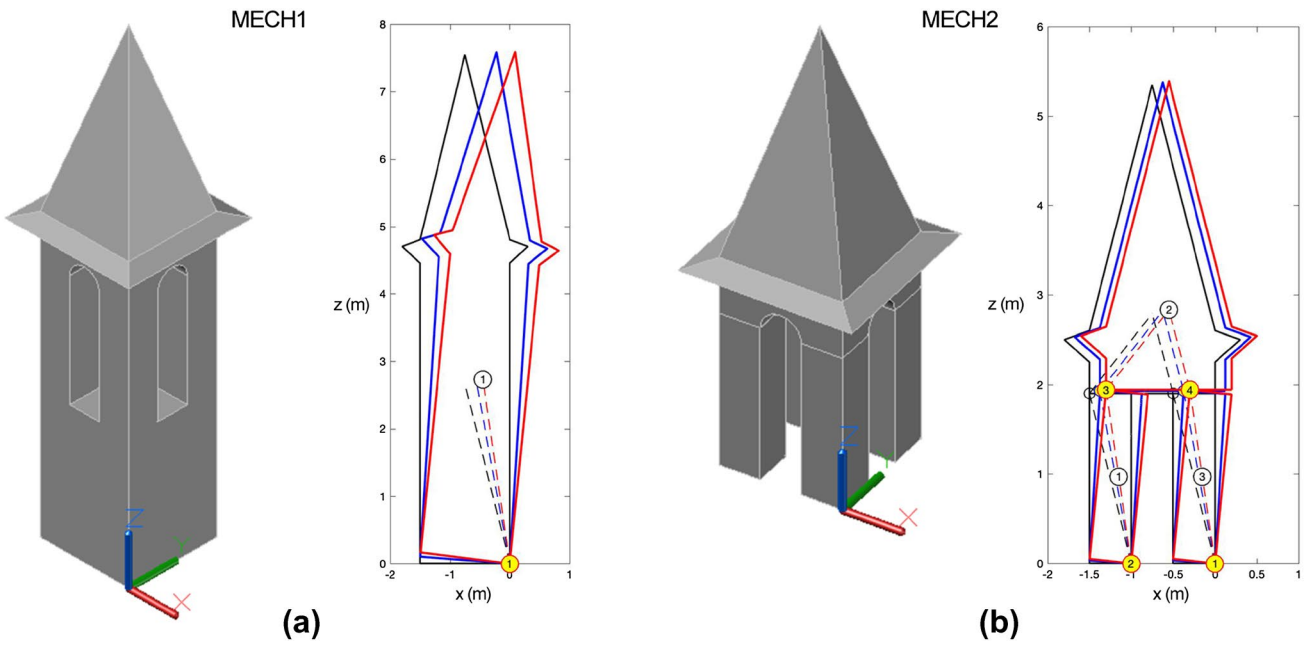

Fig. 9 Local mechanisms assessed for the pinnacles. **a** MECH1: mechanism involving the whole pinnacle with one rigid block and one hinge at the basemen; **b** MECH2: mechanism involving the upper part of the pinnacle with three rigid blocks and four hinges

Table 8 Summary of the main geometrical properties involved in the definition of the capacity curve of the pinnacle, for each considered mechanism

Mechanism	Number of blocks	Centroid coordinates (*m*)		Volume (m^3)
		x_G	y_G	
MECH1	1	−0.75	2.67	9.79
MECH2	1	−1.250	0.95	0.95
	2	−0.75	2.79	2.94
	3	−0.25	0.95	0.95

- the first, labeled "MECH1", is representative of the rocking response of the whole pinnacle around its basement (Fig. 9a) and is modeled through a single rigid block rotating around a hinge at the edge of its base;
- the second, labeled "MECH2", is representative of the rocking response of the upper part of the pinnacle around the basement of the pillars (Fig. 9b) and is modeled by three rigid blocks rotating around four hinges placed at the base and top edges of the pillars.

The similarity between the geometrical properties of the pinnacles and the double symmetry with respect to the local planes XZ and YZ (see the three-dimensional representation of Fig. 9a,b) allows, in both the considered mechanisms, a unique evaluation of the capacity that holds for all the pinnacles in each main horizontal direction and verse.

The geometrical data to be employed in the capacity evaluation have been deduced by the solid model of each block and are summarized in Table 8. Block numbering and centroid coordinates refer to the blocks and local axes of Fig. 9. Finally, the specific weight of the blocks determining the proper gravity loads is assumed to be equal to 18 kN/m^3, a conventional value for the masonry typology with bricks and lime mortar surveyed on the pinnacles.

5.2 Definition of the seismic amplification at the top of the bell tower

As anticipated, the approach adopted in the following [45] to define the seismic amplification at the top of the tower derives from the original one proposed by [61] and allows evaluating the acceleration floor spectrum $S_{eZ}(T,\xi,z)$ at different heights z of the main structure, at each level where non-structural elements under verification are placed. The floor spectrum, defined according to Eqs. (9), (10), and (11), depends among the other factors, (i) on the dynamic properties of the bell tower and (ii) on the seismic response spectrum at the base. In particular, regarding point (i), potential amplifications shall be evaluated by accounting for the natural modes of the bell tower relevant to the seismic response of the pinnacles—taking into account, if relevant, their position in the plan as well.

$$S_{eZ}(T,\xi,z) = \sqrt{\sum_k (S_{eZ,k}(T,\xi,z))^2} \geq S_e(T,\xi) \text{ for } T > T_1 \tag{9}$$

$$S_{eZ,k}(T,\xi,z) = \begin{cases} \dfrac{1.1\xi_k^{-0.5}\eta(\xi)a_{Z,k}(z)}{1+\left[1.1\xi_k^{-0.5}\eta(\xi)-1\right]\left(1-\frac{T}{aT_k}\right)^{1.6}} & T < aT_K \\ 1.1\xi_k^{-0.5}\eta(\xi)a_{Z,k}(z) \quad aT_k \leq T < bT_k \\ \dfrac{1.1\xi_k^{-0.5}\eta(\xi)a_{Z,k}(z)}{1+\left[1.1\xi_k^{-0.5}\eta(\xi)-1\right]\left(\frac{T}{bT_k}-1\right)^{1.2}} & T \geq bT_k \end{cases} \tag{10}$$

$$a_{Z,k}(z) = S_e\left(T_k,\xi_k\right)\left|\gamma_k\psi_k(z)\right|\sqrt{1+4\xi_k^2} \tag{11}$$

In particular, referring to Eqs. (9), (10), and (11):

- $S_e(T,\xi)$ is the elastic response spectrum at the base, evaluated for the equivalent period T and the equivalent viscous damping ratio ξ of the non-structural element under verification;
- $S_{eZ,k}(T_k,\xi_k,z)$ is the contribution to the floor spectrum at level z provided by the k^{th} mode of the main structure with period T_k and an equivalent viscous damping ratio ξ_k;
- a and b are coefficients defining the frequency range of maximum amplification of the floor spectrum around the period T_k, which can be assumed equal to 0.8 and 1.1, respectively (based on [61]);
- γ_k is the k^{th} modal participation coefficient;
- $\psi_k(z)$ is the k^{th} modal shape at height z (possibly corresponding to the plan position of the non-structural element);
- η is a factor correcting the elastic response spectrum for damping ratios different from 5%;
- $a_{Z,k}$ is the contribution of the k^{th} mode to the maximum peak floor acceleration.

Equation (12), thus, provides the maximum peak floor acceleration at height z, while Eq. (13) gives the contribution due to the k^{th} mode to the maximum peak of spectral acceleration in correspondence with the period T_k.

$$a_Z(z) = \sqrt{\sum_k \left(a_{Z,k}(z)\right)^2} \tag{12}$$

$$S_{eZ,k}\left(T_k,\xi,z\right) = 1.1\xi_k^{-0.5}\eta(\xi)a_{Z,k}(z) \tag{13}$$

The choice of the parameters necessary to obtain, from the above expressions, the floor spectra for each analysis

direction and each considered mechanism is further discussed here in the following.

Concerning the seismic input to be employed in the seismic assessment of mechanism MECH1, it should be specified that:

- the definition of the response spectrum at the base is described in Sect. 4.2;
- the main structure contribution, in terms of periods and mode shapes, is limited to the two first-order flexural modes acting along each main direction of the bell tower, mode B-G-Fx for the x-direction and mode B-G-Fy for the y-direction (as experimentally identified in Sect. 3.2). The corresponding modal participation coefficients were estimated according to the following expression

$$\gamma = \frac{\sum m_i \psi_i}{\sum m_i \psi_i^2} \tag{14}$$

where m_i is the mass of each horizontal sector in which the bell tower has been divided (see Sect. 4.1, Table 3), ψ_i is the modal amplitude of the experimental mode shape, eventually interpolated at the sector centroid;

- the viscous damping ratio is assumed to be identically equal to 5% since no additional dissipation is expected from the main body of the tower (which, at SLV, remains substantially in the elastic phase, see Sect. 4.2).

Instead, to define the seismic input to MECH2, the contribution of the dynamic response of each pinnacle was taken into account in addition to the one provided by the main structure. This contribution is characterized by:

- a natural period of the pinnacle assumed to be close to 0.14 s, which corresponds to the average frequency of 7 Hz experimentally identified for the pinnacles (see modes L-P identified in the range 5.5–9 Hz, Sect. 3.2);
- a modal shape extrapolated to the basement of the pillars (see Sect. 5.2) starting from the experimental one (whose maximum has been normalized to unity);
- a modal participation coefficient evaluated with Eq. (14);
- a viscous damping coefficient equal to 5%, which follows the same considerations previously discussed for mechanism MECH1.

Table 9 summarizes the values of the parameters previously discussed for both the considered mechanisms. The resulting floor spectra in the x and y directions (Fig. 10) are significantly amplified with respect to the one at the base, both in terms of peak floor acceleration (at period $T=0$ s) and maximum spectral acceleration $S_a(T)$ (at period $T=T_k$). In particular, the directional floor spectra present a single

Table 9 Parameters governing the seismic floor spectra in the assessment of pinnacles' local mechanisms

Mechanism	Level	Mode	Direction	T_k (s)	$S_a(T_k)$ (m/s^2)	γ	ψ	ξ_k	$a_{Z,k}$(m/s^2)
MECH1	L5	B-G-Fx	x	0.638	1.522	1.734	0.830	0.05	2.20
	L5	B-G-Fy	y	0.493	1.970	1.788	0.789	0.05	2.79
MECH2	L5	B-G-Fx	x	0.638	1.522	1.734	0.830	0.05	2.20
	L5	B-G-Fy	y	0.493	1.970	1.788	0.789	0.05	2.79
	L5*	L-P	x and y	0.140	2.357	1.00	1.00	0.05	2.37

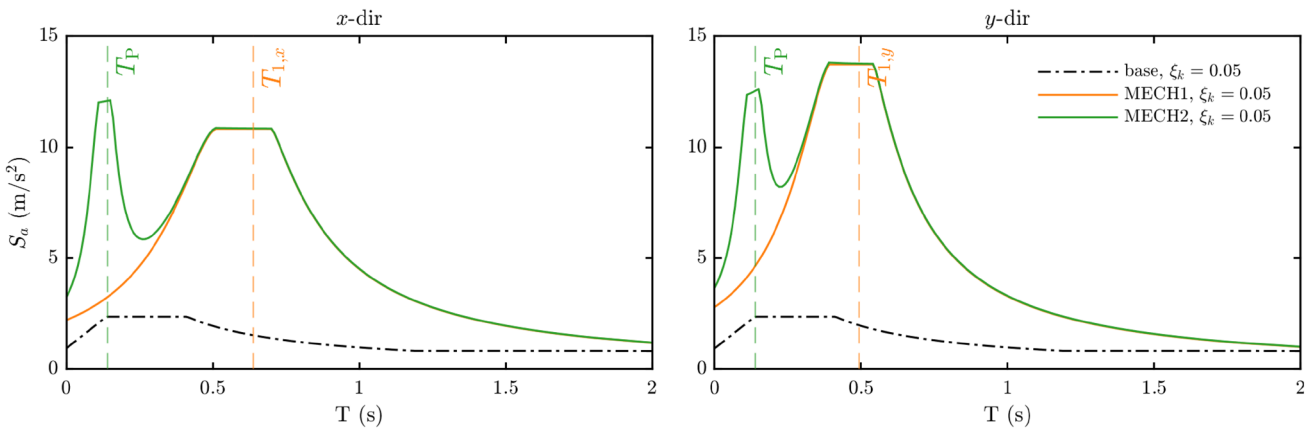

Fig. 10 Base spectrum and floor spectra in the x and y directions, as evaluated for pinnacles' local mechanisms

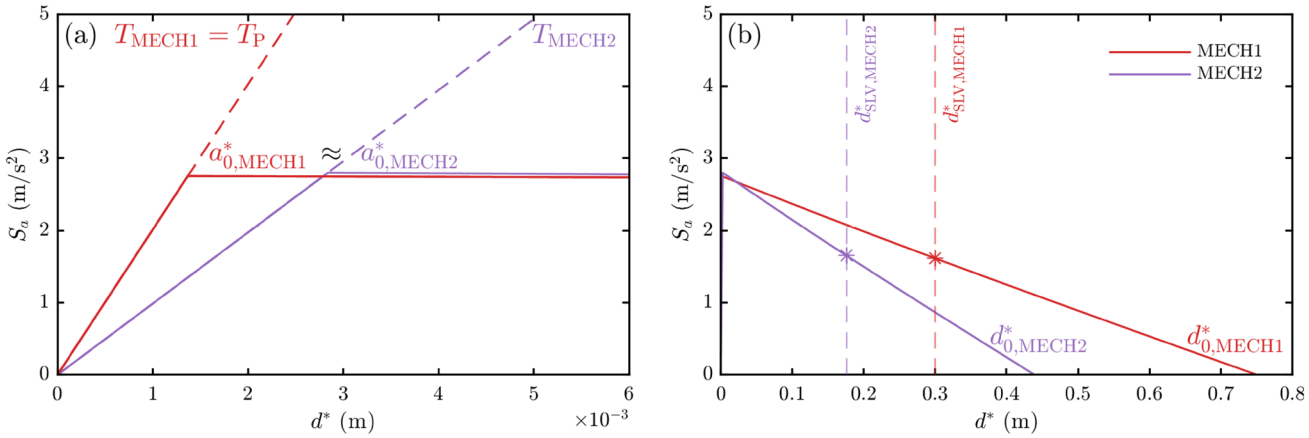

Fig. 11 Capacity curves of the pinnacles for the two examined mechanisms. **a** Initial elastic branch and activation of the mechanisms; **b** identification of SLV and ultimate displacement capacity

Table 10 Parameters governing the pinnacles' capacity curves for the two considered mechanisms

Mechanism	T_e (s)	α_0	e^*	$a_0{}^* \cong \frac{\alpha_0 g}{e^*}$ (m/s^2)	$d_0{}^*$ (m)	$d_{SLV}{}^* = 0.4\, d_0{}^*$ (m)
MECH1	0.14	0.28	1	2.76	0.750	0.30
MECH2	0.20	0.26	0.916	2.82	0.439	0.176

amplification bell in the case of MECH1, which is located around the periods of the first-order flexural modes of the bell tower in each main direction (simply $T_{1,x}$ and $T_{1,y}$ in Fig. 10). Conversely, for MECH2, the spectra exhibit an additional amplification bell caused by resonance with the pinnacle' mode of vibration (at period T_P in Fig. 10).

5.3 Results of the local seismic assessment

The comparison between the capacity curves of the two mechanisms is reported in Fig. 11, whereas Table 10 reports the defining parameters. In particular, with reference to the equivalent single-degree-of-freedom system: T_e is the initial period of the system that defines the slope of the elastic branch; α_0 is the seismic multiplier for the mechanism activation; e^* is the fraction of participant mass; $a_0{}^*$ is the spectral acceleration corresponding to the mechanism activation; $d_0{}^*$ is the ultimate displacement at the loss of static equilibrium; and $d_{SLV}{}^*$ is the capacity displacement at SLV. It can be observed that:

- the capacity curve of MECH1 is characterized by (i) an elastic branch with initial period (slope) $T_e = 0.14$ s (according to the experimental identification of Sect. 3.2) and (ii) a linearly decreasing branch with activation $a_0{}^* = 2.76$ m/s^2 (Fig. 11a) and ultimate displacement (the loss of static equilibrium) $d_0{}^* = 0.75$ m (Fig. 11b);
- the capacity curve of MECH2 is characterized by (i) an elastic branch with initial period equal to $T_e = 0.20$ s (an estimate of the pillar-spire system) and (ii) a decreasing linear branch with activation $a_0{}^* = 2.82$ m/s^2 (Fig. 11a) and ultimate displacement $d_0{}^* = 0.439$ m (Fig. 11b).

The two mechanisms are characterized by similar values of the spectral acceleration of activation $a_0{}^*$, even though the ultimate displacements $d_0{}^*$ are quite different. In particular, MECH1 is characterized by an ultimate displacement that is almost twice the one of MECH2. The capacity displacement at SLV, $d_{SLV}{}^*$ (see Sect. 5.1), is equal to 0.30 m and 0.176 m for MECH1 and MECH2, respectively.

The intersection between the capacity curves and the floor spectra (Sect. 5.2), properly scaled to the LS displacement, provides the expected peak floor acceleration. This procedure is graphically sketched in Fig. 12 for both the mechanisms involved in the assessment. The quantitative results are reported in Table 11 in terms of the safety factor $J_s = \min\left\{\frac{PFA_{SLV,x}}{PFA_x}, \frac{PFA_{SLV,y}}{PFA_y}\right\}$, which evaluates the ratio between the PFA achieving the LS displacement and the PFA at the site for the same return period. Factors lower than unity do not satisfy the verification. Although both mechanisms are verified with reference to SLV, the pinnacles are more vulnerable to MECH2 than MECH1. This result is a consequence of the lower displacement capacity $d_{SLV}{}^*$ of MECH2, being equal for both the mechanisms of the

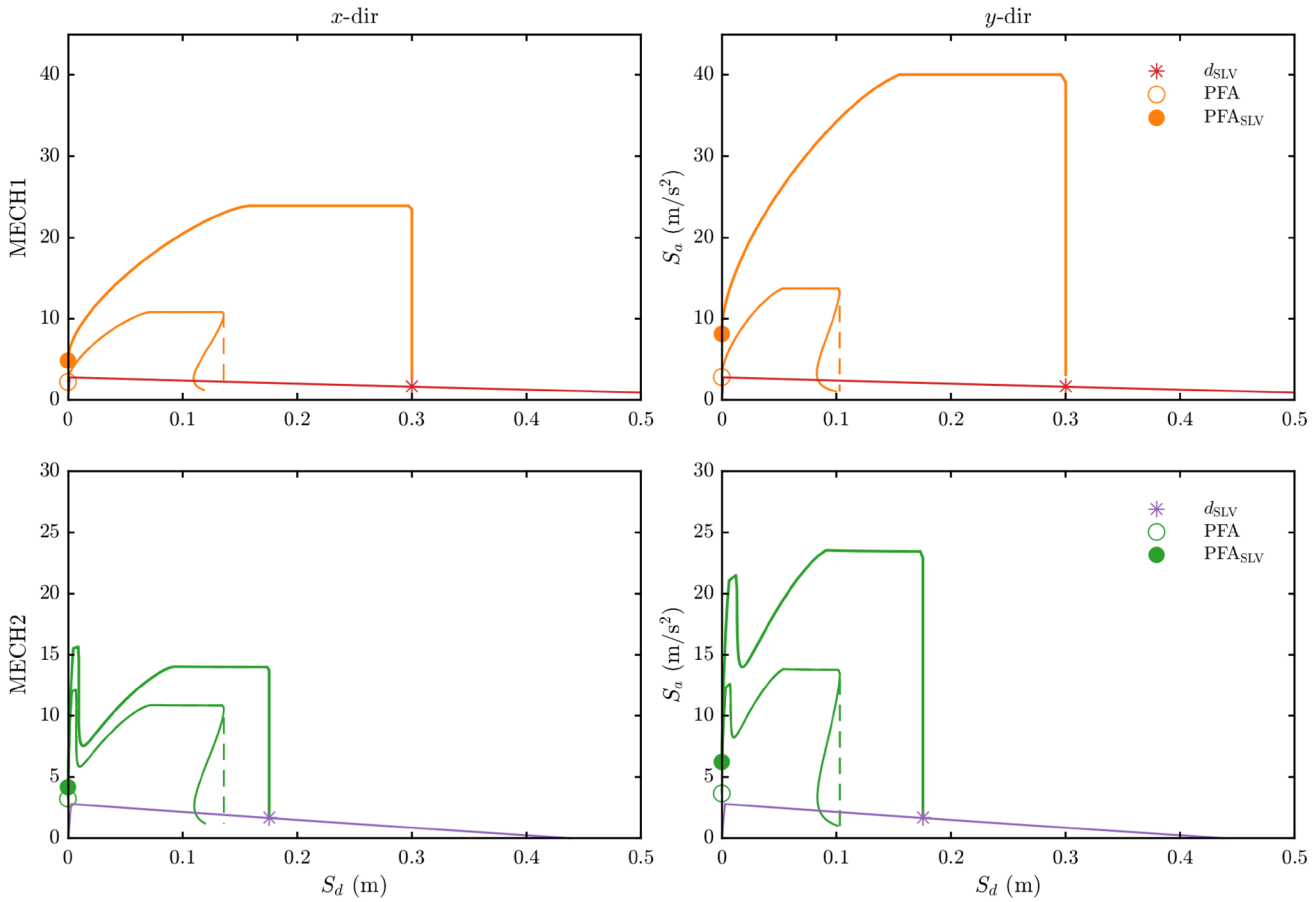

Fig. 12 Comparison between the floor spectra obtained in the two directions of analysis and the capacity curve for MECH1 and MECH2

Table 11 Results of the local seismic assessment of the pinnacles at SLV in terms of safety factor J_s

Mechanism	PFA$_x$ (m/s^2)	PFA$_y$ (m/s^2)	PFA$_{SLV,x}$ (m/s^2)	PFA$_{SLV,y}$ (m/s^2)	J_s
MECH1	2.20	2.79	4.86	8.14	2.21
MECH2	3.23	3.66	4.17	6.24	1.29

displacement demand beyond the peak of maximum spectral acceleration (dashed spectrum in Fig. 12).

6 Conclusion

The paper presents the use of AVTs to improve the reliability of seismic evaluations for the built architectural heritage, addressing the challenge to predict the seismic response and quantitatively assess the seismic performance of historical structures. In particular, the main contribution of the paper is to show how modal data identified from AVTs can be integrated into procedures prescribed by technical codes to assess the seismic safety of masonry towers. This is achieved through the discussion of a case study, the bell tower of the Saint Lawrence Cathedral in Genoa, Italy.

The seismic assessment of the tower integrates different modeling strategies and procedures. The global verification is obtained by employing a simplified mechanical cantilever model accounting for shear and flexural failures. The local verification of the pinnacles against the activation of potential out-of-plane mechanisms is achieved by employing a displacement-based approach, where a bi-linear capacity curve obtained through nonlinear kinematic analysis is compared with the seismic demand in the form of floor response spectrum. The AVTs campaign provided valuable insights into the operational dynamic behavior of the tower and pinnacles, clarifying the strong interaction with the church. This information was successfully employed, in the global assessment, to calibrate the relevant parameters on which the simplified mechanical model is based and, as the main novelty in the local verification of non-structural elements placed at the top, to accurately estimate the amplification of seismic actions due to the filter effect provided by the tower. Excluding

potential resonance phenomena between the tower and the pinnacles, this strategy provided a successful verification of the system against the seismic hazard of Genoa.

The integration of simplified mechanical modeling to study the global response of the tower with the analysis of the local mechanisms involving the out-of-plane response of the pinnacles proved to be an effective tool for a preliminary safety evaluation of the structure, being based on a limited number of parameters. In the future developments of this research, these results will be compared with those obtained by more refined nonlinear static analyses on a high-fidelity finite element model of the bell tower, calibrated in the elastic regime based on AVTs. The promising achievements of the research will, in the near future, guide the design of a possible seismic-structural health monitoring (SSHM) system for the conservation of this monument. This will allow a continuous updating of the computational models and the assessment results, providing useful data for comparing the seismic amplification at the different levels of the tower with that predicted by the expressions proposed by the technical codes, thus validating the tools today available for the seismic assessment of existing buildings.

Acknowledgements The authors gratefully acknowledge the "Soprintendenza Archeologia, Belle Arti e Paesaggio" (SABAP) of the city of Genoa, the Department of Architecture and Design (DAD) of the University of Genoa for sharing the available historical documentation on the cathedral. The authors acknowledge as well the academic spinoff "GEAmb" for providing support in the execution of ambient vibration tests on the church.

Author contributions SDA and DS: conceptualization, methodology, software, formal analysis, investigation, data curation, visualization, writing—original draft; SC and SL: methodology, software, supervision, funding, writing—review and editing. All authors read and approved the final manuscript.

Funding Open access funding provided by Università degli Studi di Genova within the CRUI-CARE Agreement.

Data availability Not applicable.

Declarations

Competing interests The authors have no relevant financial or non-financial interests to disclose. The authors have no competing interests to declare that are relevant to the content of this article.

References

1. Cattari S, Degli Abbati S, Ferretti D, Lagomarsino S, Ottonelli D, Tralli A (2014) Damage assessment of fortresses after the 2012 Emilia earthquake (Italy). Bull Earthq Eng 12(5):2333–2365. https://doi.org/10.1007/s10518-013-9520-x
2. Coïsson E, Ferretti D, Lenticchia E (2017) Analysis of damage mechanisms suffered by Italian fortified buildings hit by earthquakes in the last 40 years. Bull Earthq Eng 15(12):5139–5166. https://doi.org/10.1007/s10518-017-0172-0
3. Augenti N, Parisi F (2010) Learning from construction failures due to the 2009 L'Aquila, Italy, earthquake. J Perform Constr Facil 24(6):536–555. https://doi.org/10.1061/(ASCE)CF.1943-5509.0000122
4. Cattari S, Degli Abbati S, Ferretti D, Lagomarsino S, Ottonelli D, Rossi M, Tralli A (2012) The seismic behaviour of ancient masonry buildings after the earthquake in Emilia (Italy) on May 20th and 29th. Ingegneria Sismica 29(2–3):87–119. ISSN 0393-1420
5. Lagomarsino S (2012) Damage assessment of churches after L'Aquila earthquake (2009). Bull Earthq Eng 10(1):73–92. https://doi.org/10.1007/s10518-011-9307-x
6. Sorrentino L, Liberatore L, Decanini LD, Liberatore D (2014) The performance of churches in the 2012 Emilia earthquakes. Bull Earthq Eng 12(5):2299–2331. https://doi.org/10.1007/s10518-013-9519-3
7. Penna A, Calderini C, Sorrentino L, Carocci CF, Cescatti E, Sisti R, Borri A, Modena C, Prota A (2019) Damage to churches in the 2016 central Italy earthquakes. Bull Earthq Eng 17(10):5763–5790. https://doi.org/10.1007/s10518-019-00594-4
8. Canuti C, Carbonari S, Dall'Asta A, Dezi L, Gara F, Leoni G, Morici M, Petrucci E, Prota A, Zona A (2021) Post-earthquake damage and vulnerability assessment of churches in the Marche Region struck by the 2016 Central Italy seismic sequence. Int J Archit Heritage 15(7):1000–1021. https://doi.org/10.1080/15583058.2019.1653403
9. Ceroni F, Casapulla C, Cescatti E, Follador V, Prota A, da Porto F (2022) Damage assessment in single-nave churches and analysis of the most recurring mechanisms after the 2016–2017 central Italy earthquakes. Bull Earthq Eng. https://doi.org/10.1007/s10518-022-01507-8
10. Lagomarsino S, Podestà S (2004) Damage and vulnerability assessment of churches after the 2002 Molise, Italy, earthquake. Earthq Spectra 20(1):271–283. https://doi.org/10.1193/1.1767161
11. Lagomarsino S, Podestà S (2004) Seismic vulnerability of ancient churches: II. Statistical analysis of surveyed data and methods for risk analysis. Earthq Spectra 20(2):395–412. https://doi.org/10.1193/1.1737736
12. Fabbrocino F, Vaiano G, Formisano A, D'Amato M (2019) Large-scale seismic vulnerability and risk of masonry churches in seismic-prone areas: two territorial case studies. Front Built Environ 5:102. https://doi.org/10.3389/fbuil.2019.00102
13. Pirchio D, Walsh KQ, Kerr E, Giongo I, Giaretton M, Weldon BD, Sorrentino L (2021) Seismic risk assessment and intervention prioritization for Italian medieval churches. J Build Eng 43:103061. https://doi.org/10.1016/j.jobe.2021.103061
14. Zizi M, Rouhi J, Chisari C, Cacace D, De Matteis G (2021) Seismic vulnerability assessment for masonry churches: an overview on existing methodologies. Buildings 11(12):588. https://doi.org/10.3390/buildings11120588
15. Gattulli V, Lepidi M, Potenza F (2016) Dynamic testing and health monitoring of historic and modern civil structures in Italy. Str Monitor Maint 3(1):71. https://doi.org/10.12989/smm.2016.3.1.071

16. Clementi F, Formisano A, Milani G, Ubertini F (2021) Structural health monitoring of architectural heritage: From the past to the future advances. Int J Archit Heritage 15(1):1–4. https://doi.org/10.1080/15583058.2021.1879499
17. Ivorra S, Pallarés FJ (2006) Dynamic investigations on a masonry bell tower. Eng Struct 28(5):660–667. https://doi.org/10.1007/s10518-016-9970-z
18. Gentile C, Saisi A (2007) Ambient vibration testing of historic masonry towers for structural identification and damage assessment. Constr Build Mater 21(6):1311–1321. https://doi.org/10.1016/j.conbuildmat.2006.01.007
19. Foti D, Diaferio M, Giannoccaro NI, Mongelli M (2012) Ambient vibration testing, dynamic identification and model updating of a historic tower. NDT e Int 47:88–95. https://doi.org/10.1016/j.ndteint.2011.11.009
20. Pieraccini M, Dei D, Betti M, Bartoli G, Tucci G, Guardini N (2014) Dynamic identification of historic masonry towers through an expeditious and no-contact approach: Application to the "Torre del Mangia" in Siena (Italy). J Cult Herit 15(3):275–282. https://doi.org/10.1016/j.culher.2013.07.006
21. Standoli G, Giordano E, Milani G, Clementi F (2021) Model updating of historical belfries based on OMA identification techniques. Int J Archit Heritage 15(1):132–156. https://doi.org/10.1080/15583058.2020.1723735
22. Monchetti S, Viscardi C, Betti M, Bartoli G (2022) Bayesian-based model updating using natural frequency data for historic masonry towers. Probabilistic Eng Mech 70:103337. https://doi.org/10.1016/j.probengmech.2022.103337
23. de Silva F, Pitilakis D, Ceroni F, Sica S, Silvestri F (2018) Experimental and numerical dynamic identification of a historic masonry bell tower accounting for different types of interaction. Soil Dyn Earthq Eng 109:235–250. https://doi.org/10.1016/j.soildyn.2018.03.012
24. Aloisio A, Di Pasquale A, Alaggio R, Fragiacomo M (2022) Assessment of seismic retrofitting interventions of a masonry palace using operational modal analysis. Int J Archit Heritage 16(5):692–704. https://doi.org/10.1080/15583058.2020.1836531
25. Ramos LF, Marques L, Lourenço PB, De Roeck G, Campos-Costa A, Roque J (2010) Monitoring historical masonry structures with operational modal analysis: two case studies. Mech Syst Signal Process 24(5):1291–1305. https://doi.org/10.1016/j.ymssp.2010.01.011
26. Azzara RM, Girardi M, Iafolla V, Lucchesi DM, Padovani C, Pellegrini D (2021) Ambient vibrations of age-old masonry towers: Results of long-term dynamic monitoring in the historic centre of Lucca. Int J Archit Heritage 15(1):5–21. https://doi.org/10.1080/15583058.2019.1695155
27. Barsocchi P, Bartoli G, Betti M, Girardi M, Mammolito S, Pellegrini D, Zini G (2021) Wireless sensor networks for continuous structural health monitoring of historic masonry towers. Int J Archit Heritage 15(1):22–44. https://doi.org/10.1080/15583058.2020.1719229
28. Saisi A, Gentile C, Ruccolo A (2018) Continuous monitoring of a challenging heritage tower in Monza, Italy. J Civ Str Health Monit 8(1):77–90. https://doi.org/10.1007/s13349-017-0260-5
29. Kita A, Cavalagli N, Venanzi I, Ubertini F (2021) A new method for earthquake-induced damage identification in historic masonry towers combining OMA and IDA. Bull Earthq Eng 19(12):5307–5337. https://doi.org/10.1007/s10518-021-01167-0
30. Pallarés FJ, Betti M, Bartoli G, Pallarés L (2021) Structural health monitoring (SHM) and Nondestructive testing (NDT) of slender masonry structures: A practical review. Constr Build Mater 297:123768. https://doi.org/10.1016/j.conbuildmat.2021.123768
31. Zanotti Fragonara L, Boscato G, Ceravolo R, Russo S, Ientile S, Pecorelli ML, Quattrone A (2017) Dynamic investigation on the Mirandola bell tower in post-earthquake scenarios. Bull Earthq Eng 15:313–337. https://doi.org/10.1007/s10518-016-9970-z
32. Bassoli E, Vincenzi L, D'Altri AM, de Miranda S, Forghieri M, Castellazzi G (2018) Ambient vibration-based finite element model updating of an earthquake-damaged masonry tower. Str Control Health Monit 25(5):e2150. https://doi.org/10.1002/stc.2150
33. Saisi A, Gentile C (2020) Investigation Strategy for Structural Assessment of Historic Towers. Infrastructures 5(12):106. https://doi.org/10.3390/infrastructures5120106
34. D'Ambrisi A, Mariani V, Mezzi M (2012) Seismic assessment of a historical masonry tower with nonlinear static and dynamic analyses tuned on ambient vibration tests. Eng Str 36:210–219. https://doi.org/10.1016/j.engstruct.2011.12.009
35. Sabia D, Aoki T, Cosentini RM, Lancellotta R (2015) Model updating to forecast the dynamic behavior of the Ghirlandina Tower in Modena, Italy. J Earthq Eng 19(1):1–24. https://doi.org/10.1080/13632469.2014.962668
36. Ferraioli M, Miccoli L, Abruzzese D, Mandara A (2017) Dynamic characterisation and seismic assessment of medieval masonry towers. Nat Hazards 86(2):489–515. https://doi.org/10.1007/s11069-016-2519-2
37. Milani G, Clementi F (2021) Advanced seismic assessment of four masonry bell towers in Italy after operational modal analysis (OMA) identification. Int J Archit Heritage 15(1):157–186. https://doi.org/10.1080/15583058.2019.1697768
38. Brincker R, Zhang L, Andersen P (2001) Modal identification of output-only systems using frequency domain decomposition. Smart Mater Str 10(3):441. https://doi.org/10.1088/0964-1726/10/3/303
39. Pappa RS, Elliott KB, Schenk A (1993) Consistent-mode indicator for the eigensystem realization algorithm. J Guid Control Dyn 16(5):852–858. https://doi.org/10.2514/3.21092
40. Lagomarsino S, Ottonelli D, Cattari S (2015) An analytical mechanical model for the seismic assessment of bell towers. Key Eng Mater 624:97–105. https://doi.org/10.4028/www.scientific.net/KEM.624.97
41. DPCM2011 (2011) Direttiva del Presidente del Consiglio dei Ministri del 9 febbraio 2011. Valutazione e Riduzione del Rischio Sismico del Patrimonio Culturale con Riferimento alle Norme Tecniche per le Costruzioni di cui al Decreto del Ministero delle Infrastrutture e dei Trasporti del 14 gennaio 2008. Gazzetta Ufficiale Serie Generale n. 47 del 26/02/2011, Supplemento Ordinario n. 54. Available online: https://www.gazzettaufficiale.it/eli/gu/2011/02/26/47/so/54/sg/pdf (In Italian)
42. Calderini C, Cattari S, Lagomarsino S (2009) In-plane strength of unreinforced masonry piers. Earthq Eng Str Dyn 38(2):243–267. https://doi.org/10.1002/eqe.860
43. Turnšek V, Čačovič F (1971) Some experimental results on the strength of brick masonry walls. Proceedings of the 2nd International Brick Masonry Conference, Stoke-on-Trent, UK, pp. 149–156.
44. Mann W, Müller H (1980) Failure of shear-stressed masonry: an enlarged theory, tests and application to shear-walls. Proceedings of the International Symposium on Load-bearing Brickwork, London, UK, pp. 1–13
45. MIT2019 (2019) Circolare 21 gennaio 2019, n. 7 Consiglio Superiore dei Lavori Pubblici, Ministero delle Infrastrutture e dei Trasporti. Istruzioni per l'applicazione dell'«Aggiornamento delle "Norme tecniche per le costruzioni"» di cui al decreto ministeriale 17 gennaio 2018. Gazzetta Ufficiale Serie Generale n. 35 del 11/02/2019, Supplemento Ordinario n. 5. Available online: https://www.gazzettaufficiale.it/eli/gu/2019/02/11/35/so/5/sg/pdf (in Italian)
46. Regni M, Arezzo D, Carbonari S, Gara F, Zonta D (2018) Effect of environmental conditions on the modal response of a 10-story

reinforced concrete tower. Shock Vib. https://doi.org/10.1155/2018/9476146
47. Gara F, Arezzo D, Nicoletti V, Carbonari S (2021) Monitoring the modal properties of an RC school building during the 2016 Central Italy seismic swarm. J Str Eng 147(7):05021002. https://doi.org/10.1061/(ASCE)ST.1943-541X.0003025
48. Michel C, Zapico B, Lestuzzi P, Molina FJ, Weber F (2011) Quantification of fundamental frequency drop for unreinforced masonry buildings from dynamic tests. Earthq Eng Str Dynam 40(11):1283–1296. https://doi.org/10.1002/eqe.1088
49. MIT2018 (2018) Decreto Ministeriale del Ministero delle Infrastrutture e dei Trasporti del 17 gennaio 2018. Aggiornamento delle «Norme tecniche per le costruzioni». Gazzetta Ufficiale Serie Generale n. 42 del 20/02/2018, Supplemento Ordinario n. 8. Available online: https://www.gazzettaufficiale.it/eli/gu/2018/02/20/42/so/8/sg/pdf (in Italian)
50. Morandi P, Butenweg C, Breis K, Beyer K, Magenes G (2022) Latest findings on the behaviour factor q for the seismic design of URM buildings. Bull Earthq Eng 20:5797–5848. https://doi.org/10.1007/s10518-022-01419-7
51. Lagomarsino S, Ottonelli D (2012) A Macro-Block program for the seismic assessment (MBPERPETUATE). PERPETUATE-EC-FP7 Project, Deliverable D29, www.perpetuate.eu
52. Lagomarsino S, Cattari S (2015) PERPETUATE guidelines for seismic performance-based assessment of cultural heritage masonry structures. Bull Earthq Eng 13(1):13–47. https://doi.org/10.1007/s10518-014-9674-1
53. Lagomarsino S (2015) Seismic assessment of rocking masonry structures. Bull Earthq Eng 13(1):97–128. https://doi.org/10.1007/s10518-014-9609-x
54. Degli Abbati S, Cattari S, Lagomarsino S (2021) Validation of displacement-based procedures for rocking assessment of cantilever masonry elements. Structures 33:3397–3416. https://doi.org/10.1016/j.istruc.2021.04.102
55. Degli Abbati S, Lagomarsino S (2017) Out-of-plane static and dynamic response of masonry panels. Eng Str 150:803–820. https://doi.org/10.1016/j.engstruct.2017.07.070
56. Menon A, Magenes G (2011) Definition of seismic input for out of plane response of masonry walls: I. Parametric study. J Earthq Eng 15(2):165–194. https://doi.org/10.1080/13632460903456981
57. Calvi PM, Sullivan TJ (2014) Estimating floor spectra in multiple degree of freedom systems. Earthq Str 7(1):17–38. https://doi.org/10.12989/eas.2014.7.1.017
58. Baggio S, Berto L, Rocca I, Saetta A (2018) Vulnerability assessment and seismic mitigation intervention for artistic assets: from theory to practice. Eng Str 167:272–286. https://doi.org/10.1193/081017EQS159M
59. Anajafi H, Medina RA (2019) Lessons learned from evaluating the responses of instrumented buildings in the United States: the effects of supporting building characteristics on floor response spectra. Earthq Spectra 35(1):159–191. https://doi.org/10.1193/081017EQS159M
60. Derakhshan H, Nakamura Y, Griffith MC, Ingham JM (2020) Suitability of height amplification factors for seismic assessment of existing unreinforced masonry components. J Earthq Eng 26(3):1347–1366. https://doi.org/10.1080/13632469.2020.1716889
61. Degli Abbati S, Cattari S, Lagomarsino S (2018) Theoretically-based and practice-oriented formulations for the floor spectra evaluation. Earthq Str 15(5):565–581. https://doi.org/10.12989/eas.2018.15.5.565
62. Degli Abbati S, Cattari S, Lagomarsino S (2022) Validation of a practice-oriented floor spectra formulation through actual data from the 2016/2017 Central Italy earthquake. Bull Earthq Eng 20:7477–7511. https://doi.org/10.1007/s10518-022-01498-6